Materials and Design 88 (2015) 751–758

Contents lists available at ScienceDirect

Materials and Design

journal homepage: www.elsevier.com/locate/jmad

Investigation on decomposition behavior of austenite under continuous cooling in vanadium microalloyed steel (30MSV6)

Seyed Hadi Mohamadi Azghandi *, Vahide Ghanooni Ahmadabadi, Iman Raoofian, Fateh Fazeli [1], Mansour Zare, Ahad Zabett, Hamed Reihani

Department of Metallurgical and Materials Engineering, Faculty of Engineering, Ferdowsi University of Mashhad, Mashhad 91677-1111, Iran

ARTICLE INFO

Article history:
Received 3 February 2015
Received in revised form 31 July 2015
Accepted 10 September 2015
Available online 14 September 2015

Keywords:
Microalloyed steel
Austenite decomposition
Modeling
CCT
Hardness

ABSTRACT

In the present study, investigations are focused on microstructural evolution and the resulting hardness during continuous cooling transformation (CCT) in a commercial vanadium microalloyed steel (30MSV6). Furthermore, the effects of cooling rate and austenite grain size (AGS) on CCT behavior of the steel have been studied by employing high-resolution dilatometry. Quantitative metallography accompanied with scanning electron microscopy (SEM) has efficiently confirmed the dilatometric measurements of transformation kinetics and austenite decomposition products. A semi-empirical model has been proposed for prediction of microstructural development during austenite decomposition of the steel and the resultant hardness. The model consists of 8 sub-models including ferrite transformation start temperature, ferrite growth, pearlite start temperature, pearlite growth, bainite start temperature, bainite growth, martensite start temperature and hardness. The transformed fractions of ferrite, pearlite and bainite have been described using semi-empirical Johnson–Mehl–Avrami–Kolmogorov (JMAK) approach in combination with Scheil's equation of additivity. The JMAK rate parameter for bainite has been formulated using a diffusion-controlled model. Predictions of the proposed model were found to be in close agreement with the experimental measurements.

1. Introduction

Microalloyed steels were developed in the 1960s by microalloying low-carbon steels with Nb, V, and Ti in the range of 0.01 to 0.1% [1]. This type of steel has been considered as a promising alternative to quenched and tempered steel in automotive industry. Compared with conventional medium carbon steels, microalloyed steels have superior mechanical properties such as high strength and toughness in addition to their low production cost benefits [2].

Aiming to improve toughness, carbon level of microalloyed steel has been gradually reduced over the years. While compensating low amounts of carbon in this class of steels, carbide, nitride and carbo-nitride precipitates are the key factors to achieve high level of strength.

Existence of such precipitates brings about fine prior austenite grains and as a consequence leads into an ultimate fine microstructure. However, having high sensitivity to changes in microstructure, a careful control of manufacturing process is required. In this regard, deformation temperature and cooling rate are the key elements for obtaining various microstructures with resulting desirable mechanical properties [3].

Aiming at quantitatively linking the operational parameters of manufacturing process with properties of final products, considerable attention has been drawn to microstructural engineering [4–6]. For this purpose the microstructural models have recently been extended to the area of microalloyed steels [1].

As a commercial microalloyed steel, commonly used grade of 30MSV6 has been studied in several fields of manufacturing.

Rasouli et al. [7,8] studied the effect of cooling rate on microstructure and mechanical properties of 30MSV6 grade of microalloyed steel. They found that by increasing the cooling rate, the as-received ferritic–pearlitic microstructure tends to change into acicular ferrite, bainite or martensite forms. Babakhani et al. [9,10] investigated the effects of main parameters in hot forging including preheat temperature, strain and post-forging cooling rate on prior austenite grain size and mechanical properties of 30MSV6. They showed that any rise in preheat temperature from 1150 °C to 1300 °C and also decrease in strain would result in increase of austenite grain size.

The aim of this work is to model multistage phase transformation of 30MSV6 steel during continuous cooling from austenite phase. According to the fact that 30MSV6 steel is a common material implemented in automotive industry, developing a model to predict final mechanical properties dependent on controllable industry conditions (such as cooling rate and austenitizing temperature) and therefore to find optimized manufacturing conditions can be beneficial. Before the present study, similar models (based on Avrami equation) have been developed

* Corresponding author.
E-mail address: h.mohamadi@staff.um.ac.ir (S.H. Mohamadi Azghandi).
[1] F. Fazeli was a former faculty member of Ferdowsi University of Mashhad and he is currently with CanmetMATERIALS, National Resources Canada, Hamilton, ON, Canada.

http://dx.doi.org/10.1016/j.matdes.2015.09.046
0264-1275/

for other kinds of steels except for 30MSV6 steel. In the current study, phase transformation constants which are necessary for transformation modeling have been found for the mentioned steel.

2. Experimental procedure

As-received vanadium microalloyed steel (30MSV6) samples with ferrite–pearlite microstructure (shown in Fig. 1) was supplied by Iran alloy steel Co. in a solid cylindrical form. Chemical composition of the samples is given in Table 1.

Cubic specimens ($10 \times 10 \times 10$ mm^3) were prepared for austenite grain size measurements. The samples were heated up to temperatures ranging from 950 to 1200 °C, at heating rate of 10 °C/s and held in a controlled-atmosphere tube furnace. Then the specimens were water quenched prior to ferritic transformation. These tests provided the information on proper reheating conditions for subsequent dilatometric examinations. The cubic specimens have been used only for austenite grain size evaluation.

As shown in Fig. 2, three austenitizing temperatures (i.e. 950 °C, 1050 °C and 1150 °C) and four cooling rates (i.e. 1 °C/s, 4 °C/s, 10 °C/s and 20 °C/s) are chosen which are typically applied in manufacturing practices. As shown in Fig. 2, three different prior austenite grain sizes are due to different heat treatments.

The experiments were carried out by means of Adamel-Lhomargy DT1000 high-resolution dilatometer. The samples were prepared in a tubular shape from the raw materials with dimensions of 1, 15 and 8 mm in thickness, length and outer diameter, respectively. Temperatures were measured and controlled by means of a pair of thermocouples spot-welded at center of the samples in longitudinal direction. In addition, Vickers Avery–Dension Hardness tester was employed for hardness examinations. For grain boundary revealing, the cubic specimens were polished and subsequently etched using 80 mg of $CuCl_2$ in supersaturated picric acid diluted with 100 ml of distilled water in presence of a few drops of potassium carbonate as a surface active reagent. The samples were immersed in the bath of 85 °C temperature etchant for 70 s. The microstructures of the steel were studied with the aid of an optical microscope. The austenite grain size was determined with MIP image analyzing software based on planimetric approach [11] in which, the area of the grains is measured and the mean diameter of every austenite grain (EQAD) is calculated by the following equation:

$$d_A = \sqrt{\frac{4A}{\pi}}. \tag{1}$$

The tubular specimens were ground and polished employing conventional metallographic techniques [12] and then etched using 2% nital etching solution to reveal multiphase microstructures. Lever rule is normally applied in order to calculate the final fraction of single-phase transformation product. Generally, in multiphase transformations including ferrite, pearlite, bainite, and martensite, the following assumptions are required:

(i) The concentration of carbon in austenite remains constant during ferrite transformation. Otherwise, during ferrite formation, carbon enrichment in austenite phase leads to changes in lattice parameters. As a result, austenite dilation tends to diverge from linear behavior slightly [13]. (ii) Formation of ferrite and pearlite occurs in different temperature ranges. In this case, the phase fraction can be calculated as follows [13,14]:

$$f^{\alpha} = \frac{D - D^{\gamma}}{D^{\alpha} - D^{\gamma}}, f^{\alpha} + f^{\gamma} = 1$$

$$f^{p} = \frac{D - D^{\gamma} + f^{\alpha}\left(D^{\gamma} - D^{\alpha}\right)}{D^{p} - D^{\gamma}} \tag{2}$$

where f^{α} and f^{p} denote the fraction of ferrite and pearlite; and D^{γ}, D^{α}, and D^{p} are dilations associated with austenite, ferrite, pearlite phases, respectively ("D" represents the dilation of the specimen recorded by dilatometer.).

The microstructures and precipitates were analyzed using LEO 1450 VP scanning electron microscope which was equipped with energy-disperse X-ray system (Oxford INCA 7353).

Table. 1
Chemical composition of the studied vanadium microalloyed steel.

	Element								
	C	Si	Cr	Mn	V	Ti	Cu	Ni	N
wt.%	0.274	0.48	0.22	1.5	0.12	0.02	0.12	0.05	0.01

3. Modeling

Attempts were made to model phase transformation kinetics during austenite decomposition of the microalloyed steel (30MSV6 grade). The proposing model is comprised of 8 semi-empirical sub-models; ferrite transformation start temperature, ferrite growth, pearlite start temperature, pearlite growth, bainite start temperature, bainite growth, martensite start temperature and room-temperature hardness.

3.1. Ferrite transformation kinetics

3.1.1. Start temperature

Assuming that the growth of ferrite is controlled by carbon-diffusion at grain corners, the equality of two sides of the following equation

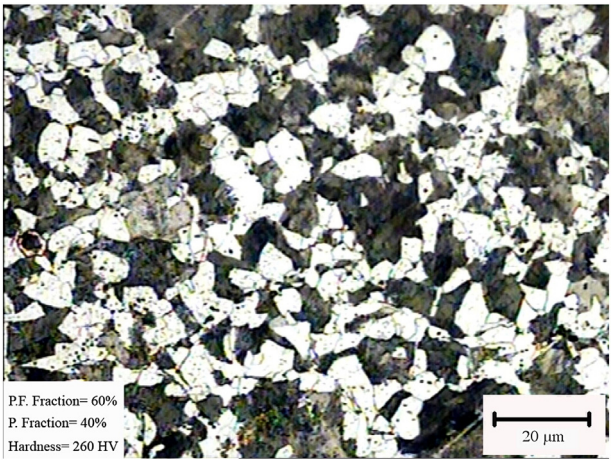

Fig. 1. Primary microstructure of as-received 30MSV6 steel.

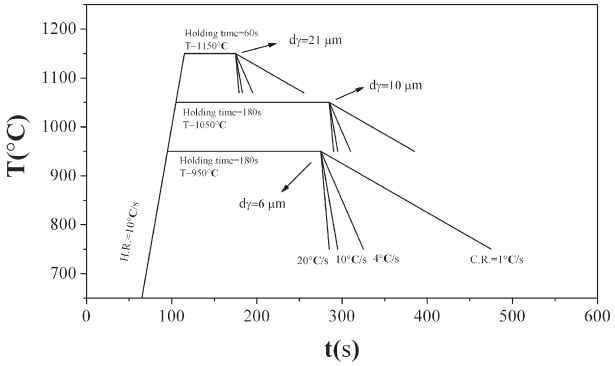

Fig. 2. Thermal plan of dilatometry tests.

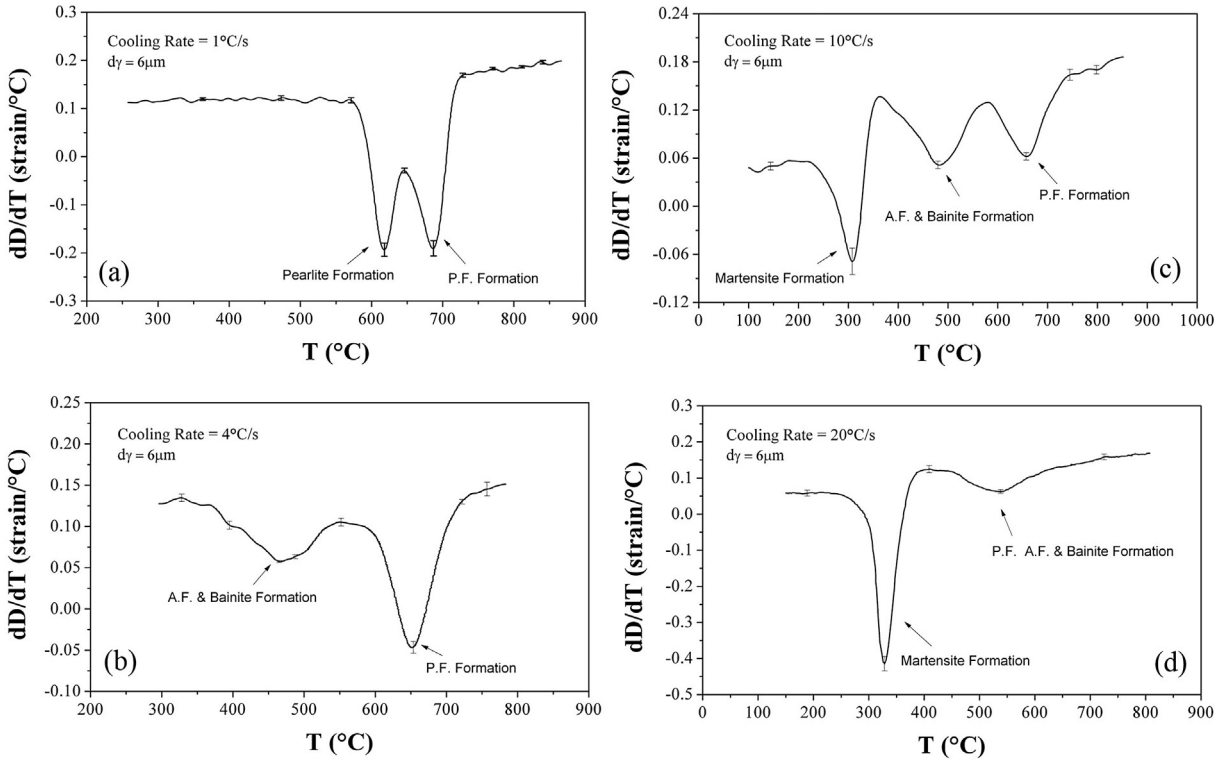

Fig. 3. The dilatometric results for the specimens with austenite grain size of 6 μm and cooling rates of (a) 1 °C/s, (b) 4 °C/s, (c) 10 °C/s, (d) 20 °C/s.

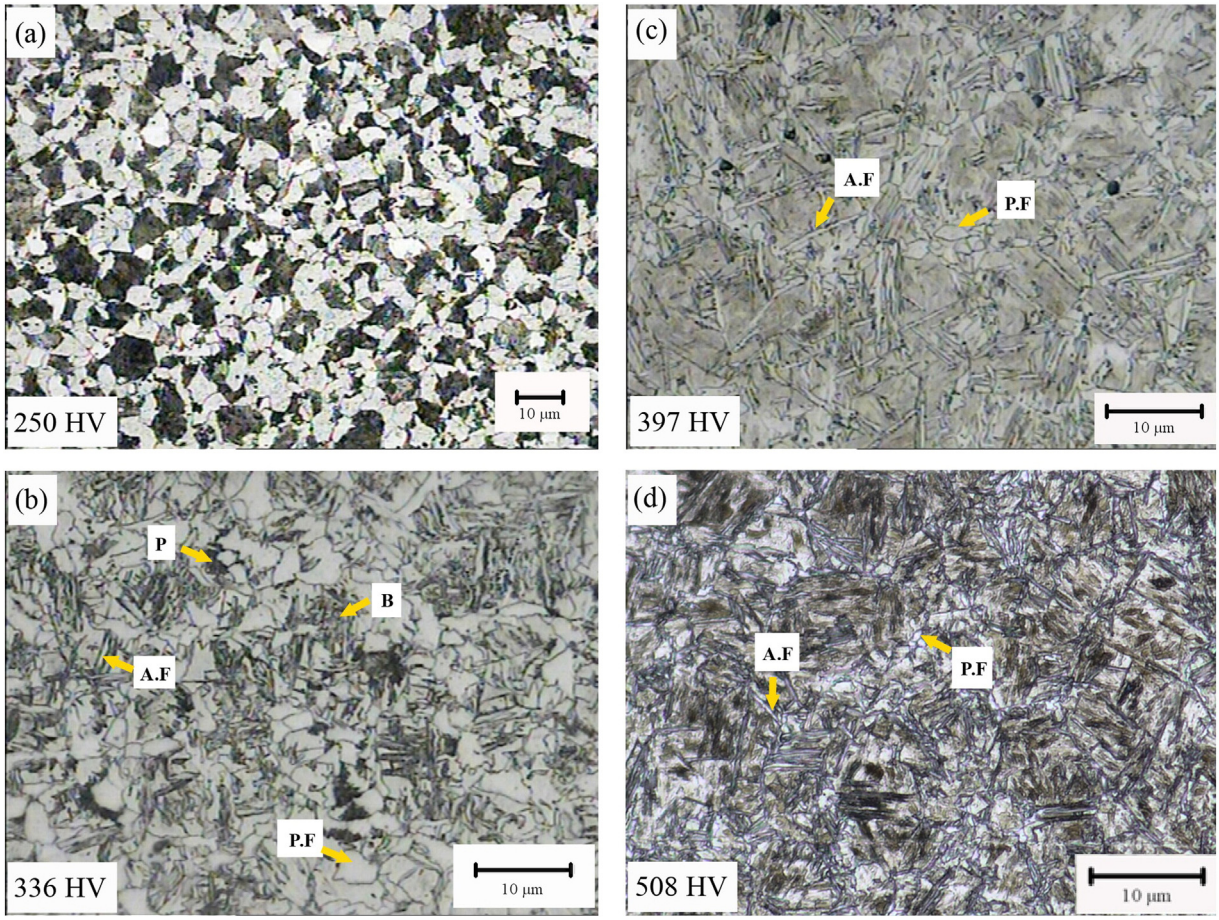

Fig. 4. The microstructure of steel sample with the initial grain size of 6 μm and cooling rates of (a) 1 °C/s, (b) 4 °C/s, (c) 10 °C/s, (d) 20 °C/s.

makes ferrite transformation start temperature be found [15]:

$$\frac{C^*-C_0}{C^{\gamma}_{eq}-C_0}=\frac{2}{\phi^{1/2}d^{\gamma}}\sqrt{\int_{T_{S,\alpha}}^{T_N} D_C\frac{C^{\gamma}_{eq}-C_0}{C^{\gamma}_{eq}-C^{\alpha}_{eq}}dT} \tag{3}$$

where C^* denotes the critical carbon concentration in the vicinity of the growing ferrite grain, above which ferrite nucleation is prevented. The terms C_0, D_C, φ and d^{γ} indicate bulk carbon concentration, carbon diffusivity in austenite [16], constant cooling rate and prior austenite grain size, respectively. Being determined by "ThermoCalc Fe2000", $C^{\gamma}{}_{eq}$ and $C^{\alpha}{}_{eq}$ represent the equilibrium carbon concentrations in austenite and ferrite. To calculate the transformation start temperature ($T_{S,\alpha}$), nucleation temperature at grain corners (T_N) and critical carbon concentration (C^*) were estimated from the experimental data.

3.1.2. Ferrite growth

By employing Scheil's rule of additivity included in the JMAK theory, the ferrite growth was described [5,17]. The volume fraction of ferrite at each cooling step, f_{α}, can be expressed by

$$\frac{f_{\alpha}}{f^{eq}_{\alpha}}=1-\exp(-b_{\alpha}t^{n_{\alpha}}) \tag{4}$$

where $f^{eq}{}_{\alpha}$, the equilibrium ferrite fraction is described by

$$f^{eq}_{\alpha}=\frac{C^{\gamma}_{eq}-C_0}{C^{\gamma}_{eq}-C^{\alpha}_{eq}}. \tag{5}$$

The equation rate is derived from

$$\frac{df_{\alpha}}{dt}=b_{\alpha}^{1/n_{\alpha}}\cdot n_{\alpha}(1-f_{\alpha})\left[-\ln(1-f_{\alpha})^{\frac{n_{\alpha}-1}{n_{\alpha}}}\right] \tag{6}$$

where n_{α} and b_{α} represent exponent and rate parameter of the growth equation, respectively. Considering $n_{\alpha}=1$ for austenite to ferrite evolution [4], b_{α} is expressed by the following equation [18]:

$$b_{\alpha}=\exp\left[AT+\frac{B}{d^{m}_{\gamma}}\right] \tag{7}$$

wherein constants A, B and m are adjustable parameters which are determined by best fitting to the experimental data of the CCT test.

3.2. Pearlite transformation kinetics

3.2.1. Start temperature

According to the experimental results, a regression analysis was conducted to obtain an analytical expression for pearlite transformation start temperature, $T_{S,P}$, as a function of cooling rate. The best correlation is obtained from a logarithmic equation which is expressed as below [19]:

$$T_{S,P}(^{\circ}\mathrm{C})=\beta-\beta_1\log(\varphi). \tag{8}$$

3.2.2. Pearlite growth

Similar methodology was adopted to describe pearlite transformation kinetics using Eq. (7), Eq. (9) and Eq. (10).

$$\frac{f_p}{f^{eq}_{p}}=1-\exp(-b_pt^{n_p}) \tag{9}$$

$$\frac{df_p}{dt}=b_p^{1/n_p}\cdot n_p\left(1-f_p\right)\left[-\ln\left(1-f_p\right)^{\frac{n_p-1}{n_p}}\right] \tag{10}$$

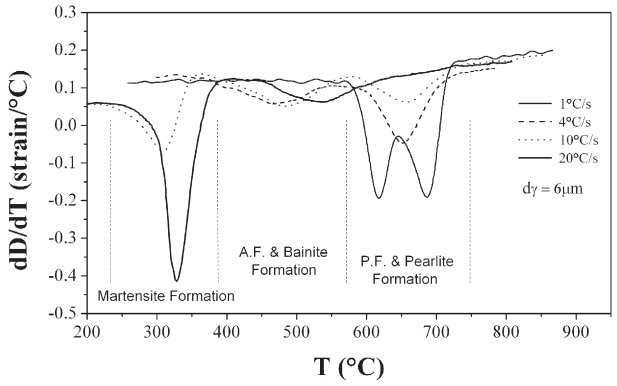

Fig. 5. Effect of cooling rate on phase transformations of austenite decomposition at prior austenite grain size of 6 μm.

However, the adjustable parameter, n_p, is calculated by best fitting to the corresponding CCT experimental results. Final pearlite fraction, $f^{eq}{}_{p}$, was also obtained from the experimental data.

3.3. Bainite transformation kinetics

3.3.1. Start temperature

Kirkaldy and Venugopalan [20] predicted the bainite start temperatures of low alloy steels, B_s, for isothermal transformation as a function of chemical composition. According to the experimental results, since B_s is not dependent on the cooling rate in the non-isothermal transformations, the Kirkaldy and Venugopalan's relation was deployed as follows:

$$B_S(^{\circ}\mathrm{C})=656-57.7\mathrm{C}-75\mathrm{Si}-35\mathrm{Mn}-15.3\mathrm{Ni}-34\mathrm{Cr}-41.2\mathrm{Mo}. \tag{11}$$

The element concentrations are in weight percent.

3.3.2. Bainite growth

For prediction of bainite transformation kinetics, a diffusion controlled model was employed to predict bainite transformation kinetics. The growth rate of bainitic plates was calculated by Zener–Hillert equation. In the equation, the maximum growth rate of the plate, $V_{\max}$, can be estimated as a function of temperature and carbon content of retained austenite by a numerical approach [21]. The normalized bainite fraction is calculated according to

$$\frac{dF_B}{dt}=K_BV_{\max}(1-F_B) \tag{12}$$

where K_B is a temperature-dependent parameter defined by the

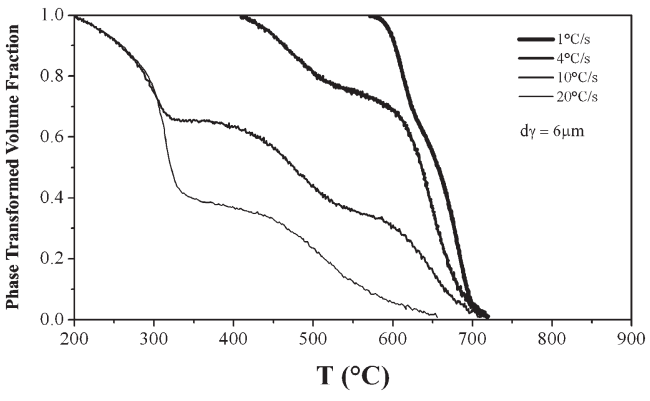

Fig. 6. Transformed fraction curves showing the effect of cooling rate on CCT behavior.

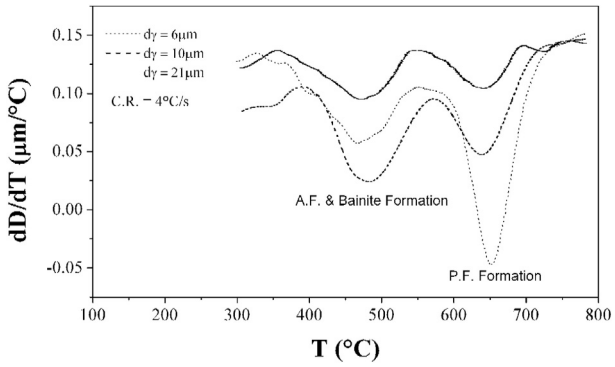

Fig. 7. Effect of prior austenite grain size on phase transformations of austenite decomposition at cooling rate of 4 °C/s.

following equation:

$$K_B = \frac{K_1}{d_{\gamma\text{-}untrans}^{K_2}} \exp\left(\frac{Q}{T}\right). \quad (13)$$

Term $d_{\gamma\text{-}untrans}$ shows the grain size of untransformed austenite at the beginning of bainite transformation which is described by $d_{\gamma\text{-}untrans} = d^{\gamma}(1-f_{\alpha})^{1/3}$. K_1, K_2 and Q are attained by fitting the Eq. (12) to the experimental bainite transformation data. Using multiplication factor, ψ (i.e. $f_B = \psi * F_B$), real bainite fraction in the final microstructure is obtained. This factor is defined by

$$\psi = \frac{C_{PE}^{\gamma} - C_0}{C_{PE}^{\gamma} - C_{PE}^{\alpha}} - f_{\alpha} \quad (14)$$

herein C^{α}_{PE} and C^{γ}_{PE} represent the para-equilibrium carbon contents of ferrite and austenite, respectively. f_{α} is the fraction of ferrite formed prior to bainite transformation.

3.4. Martensite transformation

Barbier [22] developed a model for martensite start temperature by implementing almost 1000 steels with different compositions. A developed relation of $M_{s.}$ as a function of chemical composition is expressed by

$$\begin{aligned} M_s(^{\circ}\mathrm{C}) = {} & 545 - 601.2(1 - \exp(-0.868\mathrm{C})) - 34.4\mathrm{Mn} - 13.7\mathrm{Si} - 9.2\mathrm{Cr} \\ & - 17.3\mathrm{Ni} - 15.4\mathrm{Mo} + 10.8\mathrm{V} + 4.7\mathrm{Co} - 1.4\mathrm{Al} - 16.3\mathrm{Cu} \\ & - 361\mathrm{Nb} - 2.44\mathrm{Ti} - 3448\mathrm{B} \ (\text{in wt.}\%). \end{aligned} \quad (15)$$

According to the SEM images, no considerable retained austenite was detected in the final microstructure at cooling rates of 10 and 20 °C/s. Therefore, Martensite volume fraction can be calculated as follows:

$$f_M = 1 - (f_{\alpha} + f_P + f_B). \quad (16)$$

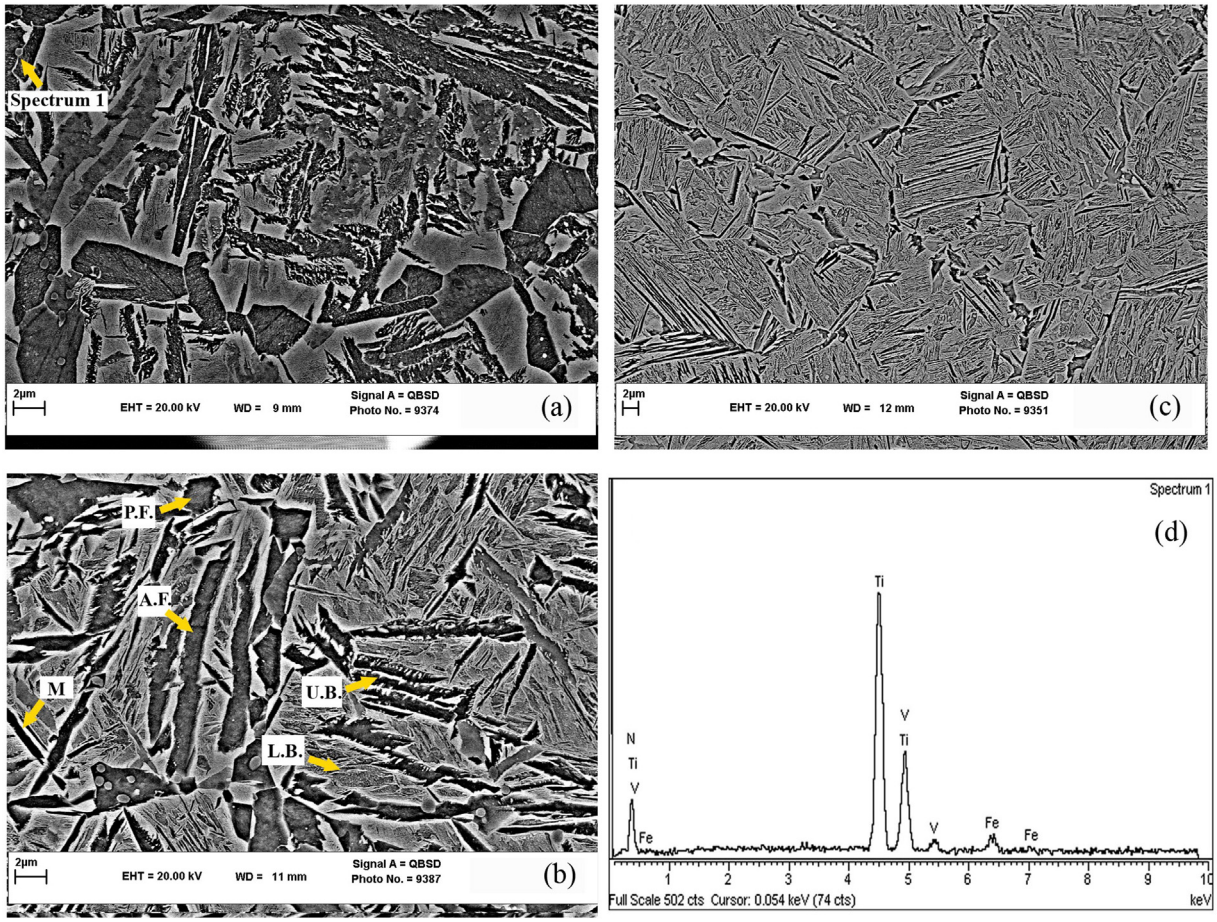

Fig. 8. SEM micrograph illustrating microstructural evolution at different cooling rates of (a) 4 °C/s, (b) 10 °C/s, (c) 20 °C/s, (d) EDX results indicating (Ti,V) carbo-nitride particle.

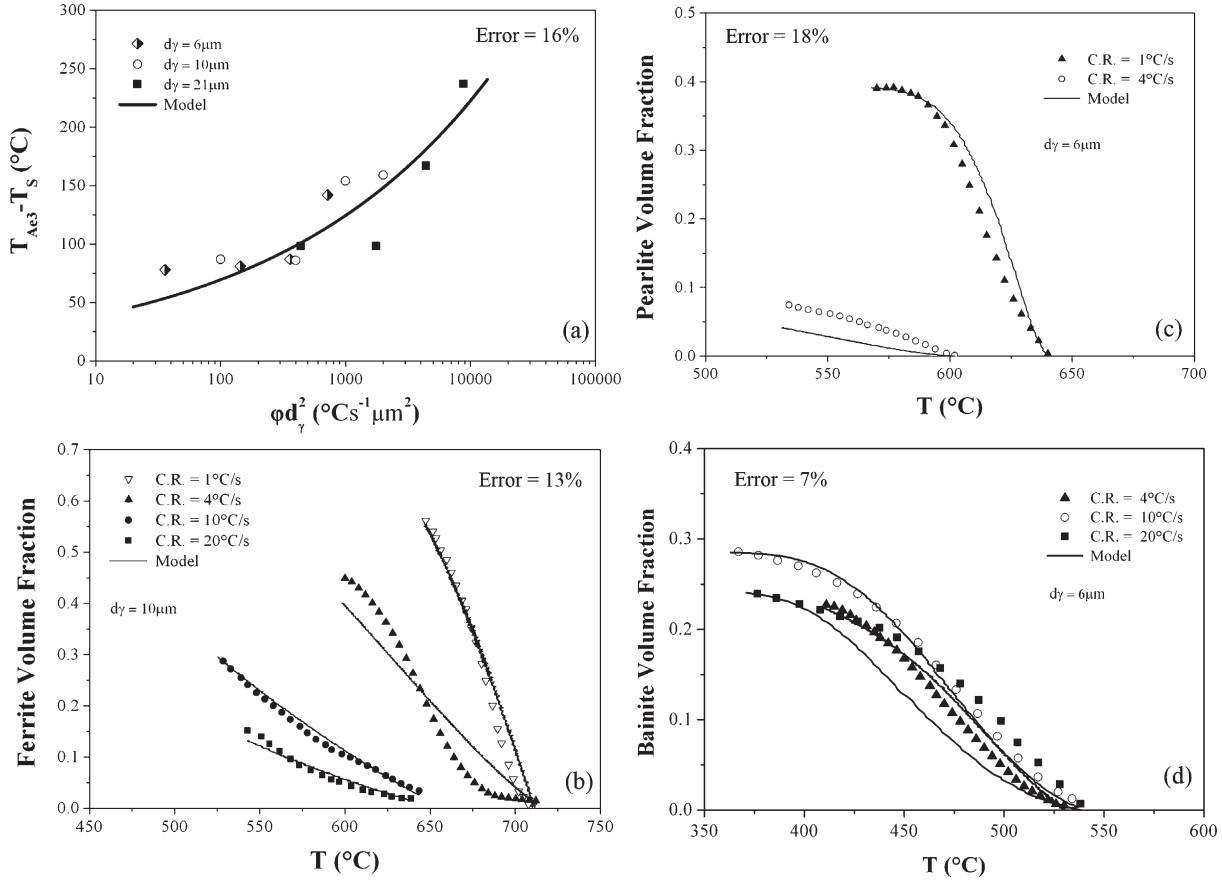

Fig. 9. Comparison of calculation and measurement results for a) ferrite transformation start temperature, b) ferrite transformation kinetics, c) pearlite transformation kinetics, d) bainite transformation kinetics.

3.5. Hardness

Hardness of the steel was calculated using the rules of mixtures:

$$H_V = (f_\alpha + f_P)H_{V,\alpha+P} + f_B H_{V,B} + f_M H_{V,M}. \quad (17)$$

Here H_V is the hardness in Vickers. f_α, f_P, f_B, and f_M are the volume fractions of ferrite, pearlite, bainite and martensite, respectively; in addition, $H_{V,\alpha+P}$, H_B and $H_{V,M}$ are the hardnesses of ferrite and pearlite mixture, bainite and martensite respectively. Empirical model of Maynier et al. [23] was used in this study for the calculation of $H_{V,\alpha+P}$, H_B and $H_{V,M}$ as a function of steel composition and cooling rate:

$$H_{V,\alpha+P} = 42 + 223C + 53Si + 30Mn + 12.6Ni + 7Cr + 19Mo + (10-19Si + 4Ni + 8Cr + 130V)\mathrm{Log}(3600 * \varphi) \quad (18)$$

$$H_{V,B} = -323 + 185C + 330Si + 153Mn + 65Ni + 144Cr + 191Mo + (89-53C-55Si-22Mn-10Ni-20Cr-33Mo)\mathrm{Log}(3600 * \varphi) \quad (19)$$

$$H_{V,M} = 127 + 949C + 27Si + 11Mn + 8Ni + 16Cr + 21\mathrm{Log}(3600 * \varphi). \quad (20)$$

In the above equations, φ is the constant cooling rate in degrees Celsius per second and the element concentrations are in wt.%.

4. Results and discussion

4.1. Experimental observations

In Fig. 2, CCT tests conducted from initial austenite microstructure of the microalloyed steel is schematically depicted. Holding time of 60 s at 1150 °C was selected instead of 180 s because of considerable grain growth at 1150 °C. The average grain size at 1150 °C after 180 s reaches more than 40 μm which is not preferable in the parts made of 30MSV6 steel in automotive industry. The results of dilatometric analysis of the samples with austenite grain size of 6 μm at different cooling rates are given in Fig. 3 (The dilatometric data is presented with the sign as a heating experiment). As it can be seen in Fig. 3-a, at cooling rate of 1 °C/s two inverse peaks are clearly seen within the temperature ranges of 650–730 °C and 590–650 °C which belong to polygonal ferrite and pearlite transformation, respectively. In Fig. 3-b, two inverse peaks are apparent at cooling rate of 4 °C/s, in which the temperature range of 650–730 °C coincides with that of polygonal ferrite transformation. Either of acicular ferrite and bainite transformations is fallen within the temperature range of 400–550 °C. Since the inverse peak on the right side is considerably larger, the majority of phase transformation

Table 2
The adjustable parameters describing transformation kinetics of austenite to ferrite and pearlite.

Austenite-to-ferrite transformation constants				Austenite-to-pearlite transformation constants			
A_1	B_1	n_α	m_α	A_2	B_2	n_p	m_p
−0.0041	−3.659	1	9.217	−0.0055	2	1.5	2

Table. 3
Comparison between measured and calculated start temperature of bainite and martensite transformations.

	B_s (°C)	M_s (°C)
Measured	540	360
Calculated	542.8	355.5
Error	0.05%	1%

corresponds to the formation of polygonal ferrite. At cooling rate of 10 °C/s, three regions are obviously shown in Fig. 3-c indicating from right to left the transformations of austenite to polygonal ferrite, mixture of acicular ferrite and bainite and finally martensite, respectively (Confirmed by Fig. 4c). The inverse peak at the right side is located within temperature range of 600–730 °C indicating transformation of austenite to polygonal ferrite. The second one refers to acicular ferrite and bainite transformation occurred at the temperature range of 400–550 °C, simultaneously. The greater intensity of the third inverse peak compared to that of ferrite and bainite phases is referred to a greater change in the lattice structure during austenite to martensite transformation [14,24]. Fig. 3-d shows two inverse peaks at cooling rate of 20 °C/s that one of them is located within the temperature range of 450–660 °C. It is a well-known fact that bainite transformation occurs below 550 °C [25]. Hence, the inverse peak can represent the ferrite and bainite transformations. Later on, the assumption made was confirmed by metallographic results (Fig. 4-d). In Fig. 3-d, the other inverse peak is attributed to martensite transformation within 250 to 360 °C; the martensite start temperature (M_S) has been measured to be 360 °C.

By employing quantitative metallography, transformation products suggested by dilatometric data were studied and their corresponding fractions were validated.

Fig. 4 gives some examples of the microstructures resulted of the CCT tests shown in Fig. 3.

The resulting austenite transformation occurred at cooling rate of 1 °C/s is asserted by the microstructure of ferrite and pearlite shown in Fig. 4-a. Presence of polygonal ferrite, acicular ferrite and bainite in the matrix is consistent with the dilatometric results achieved at cooling rate of 4 °C/s (Fig. 4-b). In Fig. 4-b, pearlite colonies are scattered through the matrix, however, due to low percentage of pearlite, they could not be detected by dilatometry (Fig. 3-b). Therefore, the following methodology was adopted to estimate kinetics of pearlite transformation at cooling rate of 4 °C/s:

(a), Final fraction of polygonal ferrite was measured based on quantitative metallography approach.
(b), Fraction of overall transformation, i.e., (ferrite + pearlite) was obtained using dilatometric data (Fig. 6). Phase fraction of pearlite was calculated by subtraction of two above fractions ((a) and (b)) from each other.

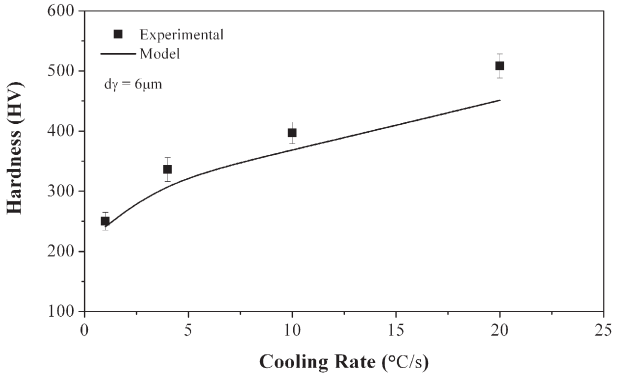

Fig. 10. Comparison of calculated and measured hardness.

In order to estimate the transformation kinetics of ferrite and bainite, similar methodology was adopted for calculation of bainite fraction from quantitative metallography and dilatometric data at 20 °C/s.

Referring to Fig. 5, the dependency of different phase formations to altering cooling rates are depicted. It is shown that by increasing the cooling rate, the intensity of polygonal ferrite formation is being depressed indicating a significant decrement of its volume. By upward trend of cooling rate up to 20 °C, simultaneous bainite and acicular ferrite formation is not considerably affected in contrast to martensite formation which is significantly intensified.

Fig. 6 depicts experimental total fraction of transformed phase showing the effect of cooling rate on CCT behavior of austenite with an initial austenite grain size of 6 μm under different cooling rates of 1, 4, 10 and 20 °C/s. In Fig. 6, multistage transformations corresponding to formation of complex microstructures such as ferrite, pearlite and bainite can be observed. According to the figure, as cooling rate ascends, the ferrite transformation start descends nearly 70 °C and also the fraction of ferrite decreases. This is completely consistent with optical microscopy results showing the obtained fraction of polygonal ferrite decreases from 0.57 to 0.15 as the cooling rate increases from 1 °C/s to 20 °C/s (Fig. 4).

Fig. 7 reveals the effect of prior austenite grain size on polygonal ferrite transformation, implying that any increase in austenite grain size leads to a noticeable reduction in polygonal ferrite fraction. Nucleation of polygonal ferrite at unstable positions such as grain boundaries can explain reasons, the fraction of polygonal ferrite tends to increase with reduction of prior austenite grain size [26].

The result of studying microstructures obtained from CCT tests (shown in Fig. 4) using SEM and energy dispersive x-ray analysis (EDX) is illustrated in Fig. 8. In Fig. 8-a, multiphase evolution of austenite to final products including polygonal ferrite (P.F.), acicular ferrite (A.F.) and upper and lower bainite (U.B. and L.B.) is apparent after cooling the sample at rate of 4 °C/s.

This is a well-established fact that precipitates function as desirable nucleation sites for acicular ferrite transformation [2,27–29]. A typical non-metallic precipitate is highlighted in Fig. 8-a, wherein it is able to act as a nucleation site for acicular ferrite phase. The results of EDX analysis indicate that the existing non-metallic precipitates have a relative composition of (Ti,V)(C,N). However, one should note that there might be possible of overlaps/interference between K lines of the C and N elements and those L lines of Ti and V thus the associated peaks are suggested to be quite speculative. From Fig. 8-b, it is observed that other than acicular ferrite and bainite (upper and lower) phases, martensite lathes are evident at cooling rate of 10 °C/s. By raising cooling rate up to 20 °C/s the volume fraction of martensite lathes increases as is shown in Fig. 8-c.

4.2. Transformation kinetics of austenite decomposition

The results of the proposed model for calculating the kinetics of austenite decomposition to ferrite, pearlite and bainite phases for different cooling rates and austenite grain sizes are depicted in Fig. 9. Modeling results for start temperature of austenite-to-ferrite transformation, $T_{s,\alpha}$, as a function of cooling rate and effective austenite grain size are illustrated in Fig. 9-a. By assuming $T_N = 760$ and $C^*/C_0 = 1.6$, a satisfactory prediction for Ts was achieved. The calculated and experimental data for volume fraction of ferrite at different cooling rates are compared in Fig. 9-b. Considering the adjustable parameters summarized in Table 2, best fit to the experimental data was attained. As can be seen in Fig. 9-b, except for the calculated results at cooling rate of 4 °C/s that slightly diverge from the experimental findings, the proposed model shows satisfactory convergence to experimental data. The best correlation between the experimental and calculated onset temperature of pearlite transformation, $T_{s,p}$, was achieved by assuming $\beta = 640$ and $\beta_1 = 58$. Observed and predicted values of pearlite volume fraction obtained by the proposed model under cooling rates of 1 °C/s

and 4 °C/s for grain size of 6 μm are given in Fig. 9-c. Taking into account the adjustable parameters given in Table 2 as pearlite transformation kinetics, the predicted values for pearlite volume fraction are to a great extent set to the experimental data, which confirms the accuracy of proposed model.

From Table 3, the modeling results of start temperature of bainite and martensite transformations are in close agreement with the experimental data.

Fig. 9-d shows the predicted and the experimental data for the volume fraction of bainite formed through different cooling paths. Equation constants (i.e. $K_1 = 2.313 * 10^{-6}$, $K_2 = 0.368$ and $Q = 15{,}011$ J/mol) are taken to achieve the best fit to experimental data. The final fraction of bainite resulting from austenite decomposition is successfully estimated by the proposed model. Errors of the sub-models are also indicated in Fig. 9. According to Fig. 10, the calculated hardness is conforming to measurements with error of 7%.

5. Conclusions

In the current paper, it has been tried to study the microstructural evolution of vanadium microalloyed steel (30MSV6) resulting from austenite decomposition during continuous cooling. The following conclusions can be made from the study:

- The CCT behavior of the steel showed a multistage transformation resulting to formation of complex microstructures such as ferrite, pearlite, bainite and martensite. Appearing of acicular ferrite at cooling rates higher than 1 °C/s was confirmed, which was found to be accompanied by polygonal ferrite, pearlite and bainite at 4 °C/s; and by polygonal ferrite, bainite and martensite at 10 °C/s and 20 °C/s.
- With increasing the cooling rate from 1 °C/s to 20 °C/s, the polygonal ferrite transformation commencement was retarded to lower temperatures and its final volume fraction decreased noticeably. The martensite temperature start (M_S) of 360 °C was achieved.
- As the prior austenite grain size increased from 6 to 21 μm, the polygonal ferrite fraction reduced considerably.
- Transformation kinetics of austenite to polygonal ferrite, pearlite and bainite during CCT were predicted by semi-empirical modeling approach. The modeling results including start temperature of polygonal ferrite, pearlite, bainite and martensite and polygonal ferrite, pearlite and bainite phase fractions and their final hardness were in close agreement with the experimental findings.
- Final microstructure and hardness of the microalloyed steel (30MSV6) are predictable for different cooling rates and austenite grain sizes by using the present model.

Acknowledgments

The authors acknowledge Dr. M. Mazinani and H. Naji for their help with technical details of the present research. Furthermore, we would like to thank Nahamin Pardazan Asia Co. for their assistance to use MIP, image analyzer software.

References

[1] T. Gladman, The Physical Metallurgy of Microalloyed Steels, Institute of Materials, United Kindom, 1997.
[2] H. Bhadeshia, R. Honeycombe, Steels: Microstructure and Properties, Elsevier Science, 2006.
[3] D.J. Naylor, Microalloyed forging steels, Mater. Sci. Forum 284–286 (1998) 83–94.
[4] D. Liu, F. Fazeli, M. Militzer, W.J. Poole, A microstructure evolution model for hot rolling of a Mo-TRIP steel, Metall Mater Trans A 38 (2007) 894–909.
[5] M. Militzer, E.B. Hawbolt, T.R. Meadowcroft, Microstructural model for hot strip rolling of high-strength low-alloy steels, Metall Mater Trans A 31 (2000) 1247–1259.
[6] X. Chun, Q. Sun, X. Chen, Research on transformation mechanism and microstructure evolution rule of vanadium–nitrogen microalloyed steels, Mater Design 28 (2007) 2523–2527.
[7] D. Rasouli, S.H. Khameneh Asl, A. Akbarzadeh, G.H. Daneshi, Effect of cooling rate on the microstructure and mechanical properties of microalloyed forging steel, J Mater Process Tech 206 (2008) 92–98.
[8] R.D. Khameneh, S.H. Asl, A. Akbarzadeh, G.H. Daneshi, Optimization of mechanical properties of a micro alloyed steel, Mater Design 30 (2009) 2167–2172.
[9] A. Babakhani, S.M.R. Ziaei, A.R. Kiani-Rashid, Investigation on the effects of hot forging parameters on the austenite grain size of vanadium microalloyed forging steel (30MSV6), J Alloy Compd 490 (2010) 572–575.
[10] A. Babakhani, A.R. Kiani-Rashid, S.M.R. Ziaei, The microstructure and mechanical properties of hot forged vanadium microalloyed steel, Mater. Manuf. Process. 27 (2011) 135–139.
[11] Annual Book of ASTM Standard, Vol. 3.01, ASTM Standard Designation, E112-88, PA: ASTM Philadelphia; 1994, p. 227.
[12] A.S.M. Handbook, Metallography and Microstructures, 2nd ed., 9, Materials Park, OH, ASM International, 2004.
[13] D.W. Suh, C.S. Oh, H.N. Hun, S.J. Kim, Dilatometric analysis of austenite decomposition considering the effect of non-isotropic volume change, Acta Mater. 55 (2007) 2659–2669.
[14] T.A. Kop, J. Sietsma, S. Van Der Zwaag, Dilatometric analysis of phase transformations in hypo-eutectoid steels, J. Mater. Sci. 36 (2001) 519–526.
[15] M. Militzer, R. Pandi, E.B. Hawbolt, Ferrite nucleation and growth during continuous cooling, Metall Mater Trans A 27 (1996) 1547–1556.
[16] J. Ågren, A revised expression for the diffusivity of carbon in binary Fe–C austenite, Scripta Metall 20 (1986) 1507–1510.
[17] P.R. Rios, Relationship between non-isothermal transformation curves and isothermal and non-isothermal kinetics, Acta Mater. 53 (18) (2005) 4893–4901.
[18] M. Umemoto, N. Komatsubara, I. Tamura, Prediction of hardenability effects from isothermal transformation kinetics, J Heat Treating 1 (1980) 57–64.
[19] T.T. Pham, E.B. Hawbolt, J.K. Brimacombe, Predicting the onset of transformation under noncontinuous cooling conditions: part II. Application to the austenite pearlite transformation, Metall Mater Trans A 26 (1995) 1993–2000.
[20] J.S. Kirkaldy, D. Venugopalan, in: A.R. Marder, J.I. Goldstein (Eds.), Phase transformations in ferrous alloys, TMS-AIME, Warrendale 1984, p. 125.
[21] F. Fazeli, M. Militzer, Phase transformations in an advanced high-strength mo-trip steel, in: J.M. Howe, D.E. Laughlin, J.K. Lee, D.J. Srolovitz, U. Dahmen (Eds.), Solid–Solid Phase Transformations in Inorganic Materials, TMS, Warrendale 2005, pp. 835–841.
[22] D. Barbier, Extension of the martensite transformation temperature relation to larger alloying elements and contents, Adv. Eng. Mater. 16 (2014) 122–127.
[23] P. Maynier, J. Dollet, P. Bastien, in: D.V. Doane, J.S. Kirkaldy (Eds.), Hardenability Concepts with Applications to Steels, AIME, New York 1978, pp. 518–544.
[24] N.N. Rammo, O.G. Abdulah, A model for the prediction of lattice parameters of iron–carbon austenite and martensite, J Alloy Compd 420 (2006) 117–120.
[25] H. Kumar, H. Bhadeshia, Bainite in Steels: Transformation, Microstructure and Properties, IOM Communications, 2001.
[26] D.A. Porter, K.H. Easterling, Phase Transformations in Metals and Alloys, 3rd ed. Taylor & Francis, 1992.
[27] I. Madariaga, I. Gutiérrez, C. Garcia-de Andrés, C. Capdevila, Acicular ferrite formation in a medium carbon steel with a two stage continuous cooling, Scripta Mater 41 (1999) 229–235.
[28] M. D'iaz Fuentes, I. Gutiérrez, Analysis of different acicular ferrite microstructures generated in a medium-carbon molybdenum steel, Mat Sci Eng A 363 (2003) 316–324.
[29] S.S. Babu, The mechanism of acicular ferrite in weld deposits, Curr Opin Solid St M 8 (2004) 267–278.